Journal of Catalysis **190,** 49–59 (2000)
doi:10.1006/jcat.1999.2711, available online at http://www.idealibrary.com on IDEAL®

Comparison of Pd/(Bulk SiC) Catalysts Prepared by Atomic Beam Deposition and Plasma Sputtering Deposition: Characterization and Catalytic Properties

A. Berthet,* A. L. Thomann,† F. J. Cadete Santos Aires,*,[1] M. Brun,* C. Deranlot,* J. C. Bertolini,* J. P. Rozenbaum,† P. Brault,† and P. Andreazza‡

*Institut de Recherches sur la Catalyse (UPR 5401-CNRS), Conventionné à l'Université Claude Bernard Lyon 1, 2, avenue Albert Einstein, F-69626 Villeurbanne Cedex, France; †Groupe de Recherches sur l'Energétique des Milieux Ionisés, Faculté des Sciences, CNRS Université Orléans, B.P. 6759, F-45067 Orléans Cedex 2, France; and ‡Centre de Recherche sur la Matière Divisée, CNRS, 1B rue de la Férollerie, F-45071 Orléans Cedex 2, France

Received July 15, 1999; revised September 21, 1999; accepted September 27, 1999

Pd on SiC catalysts have been prepared using two different physical processes: atomic beam deposition (ABD) and plasma sputtering deposition (PSD). Whatever the method, Pd deposition (ranging between 0.3 and about 12 monolayer equivalent) yields thin metal adlayers. However, the catalysts prepared by ABD exhibit a 2D-like growth, with a strong metal support interaction which remains even for the highest Pd contents investigated. At lower Pd content the presence of adatoms and/or small nuclei in strong interaction with the SiC support is evidenced for samples prepared by PSD; but increasing the Pd content of PSD samples yields a rapid growth of 3D Pd particles which have the typical properties of bulk palladium. While the ABD catalysts exhibit good activity toward the 1,3-butadiene hydrogenation reaction, whatever the Pd content, PSD catalysts with low Pd content were quite inactive and/or strongly deactivated. However, at higher Pd content the PSD technique produces rather good catalysts.

Key Words: **palladium; silicon carbide; catalysts; atomic beam deposition; low-pressure plasma sputtering; 1,3-butadiene hydrogenation.**

INTRODUCTION

Silicon carbide (SiC) is a refractory material that has a high thermal conductivity. As already mentioned (1), the SiC thermal conductivity, 500 W/mK for the single crystal state at room temperature, is close to that of metals such as Ag or Cu (400–500 W/mK). Therefore, by favoring the dissipation of the heat produced by very exothermic reactions, an improvement in the Pd reactivity (activity and also selectivity) can be expected. On SiC, the low content of anchoring sites (OH groups, etc.) makes metal deposition by chemical methods difficult. Therefore, two physical processes for the metal deposition have been attempted: atomic beam deposition (2) and plasma sputtering deposition (3). Since, in the plasma process, the substrate is submitted to low-energy ion bombardment during deposition, it is expected that the film growth will be rather different.

In the following we present:

(i) the characterization of the Pd/SiC catalysts obtained according to these two ways of elaboration, with the use of Auger electron spectroscopy (AES), X-ray photoelectron spectroscopy (XPS), transmission electron microscopy (TEM), tapping mode atomic force microscopy (TMAFM), and grazing incidence small angle X-ray scattering (GISAXS).

(ii) the catalytic properties of these samples with respect to the 1,3-butadiene hydrogenation, a quite exothermic reaction ($\Delta H^0_{298} = -56.51$ kcal mol^{-1}), working generally with a very high turnover frequency (TOF).

The results are discussed in terms of both Pd deposit morphology and properties in relation to the physical method of preparation.

EXPERIMENTAL

(a) The Bulk SiC Support

The bulk SiC support (small plates of 1 cm × 1 cm × 0.1 cm) was purchased from Morton Advanced Materials (USA). It is a polycrystalline silicon carbide, prepared by CVD, which has a low temperature form (<1500° C) with cubic β-SiC structure. It has very high purity (>99.9995%) and high chemical resistance. Its thermal conductivity is higher than 300 W/mK.

Before use, the SiC samples are polished with a diamond paste particle size down to 0.1 μm, ultrasonically cleaned in ethanol, and wiped with a soft paper soaked with ethanol, in order to eliminate particles formed during the polishing. After this preparation only some grooves are present on the surface as observed on AFM pictures (Fig. 1).

[1] To whom correspondence should be addressed. Fax: 33-4 72 44 53 99. E-mail: aires@catalyse.univ-lyon1.fr.

0021-9517/00 $35.00

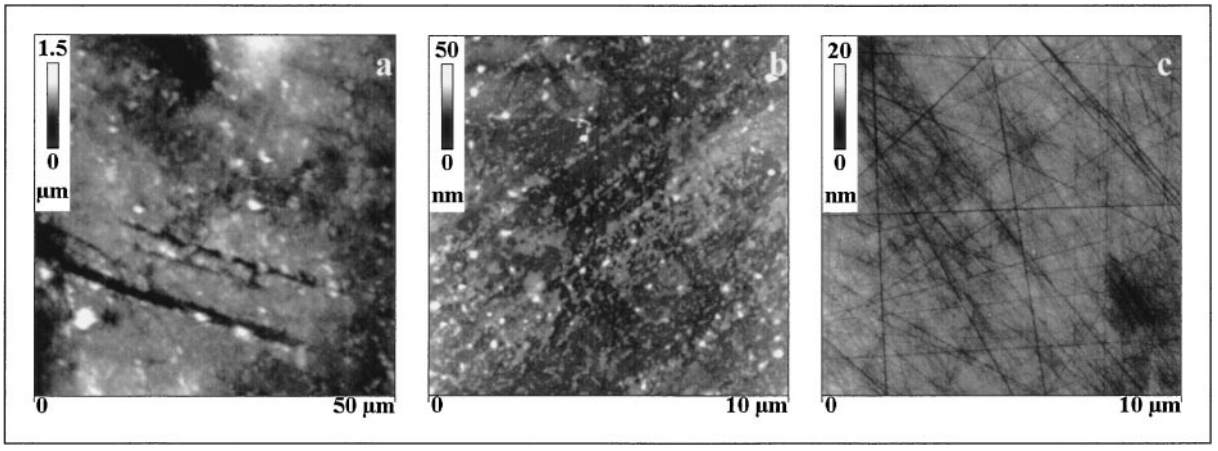

FIG. 1. Large-scale TMAFM images of the SiC support surface before polishing (a), after polishing and ultrasonically cleaning (b), and after polishing, ultrasonically cleaning, and ethanol-soaked tissue rubbing (c).

The Auger spectrum of the β-SiC support, after cleaning by argon ion bombardment and further heating, is shown in Fig. 2. The peaks at 92 and 272 eV are attributed to the KLL and $L_{2,3}VV$ Auger transitions respectively of Si and C atoms in SiC. The presence of some oxygen is evidenced by the additional peak visible at 510 eV (O KLL Auger transition).

The XPS Si 2p and C 1s levels show two maxima at 100.2 and 282.7 eV, characteristic respectively of the Si and C of SiC (4). The two other peaks observed for C 1s can be attributed to graphite-like carbon, which has been shown to terminate SiC surfaces (5), and to contaminant carbon (organic compounds) (6) (Fig. 3).

(b) Pd Catalysts Obtained by Plasma Sputtering Deposition (PSD)

The reactor is shown in Fig. 4. A high-frequency (100 MHz) plasma is initiated in argon gas (100 mTorr pressure) with an input power of several watts. The metal atom source is a helical wire which is negatively biased (−100 V) with respect to the plasma potential (≈80 V) so that Ar^+ ions present in the plasma are attracted and gain sufficient

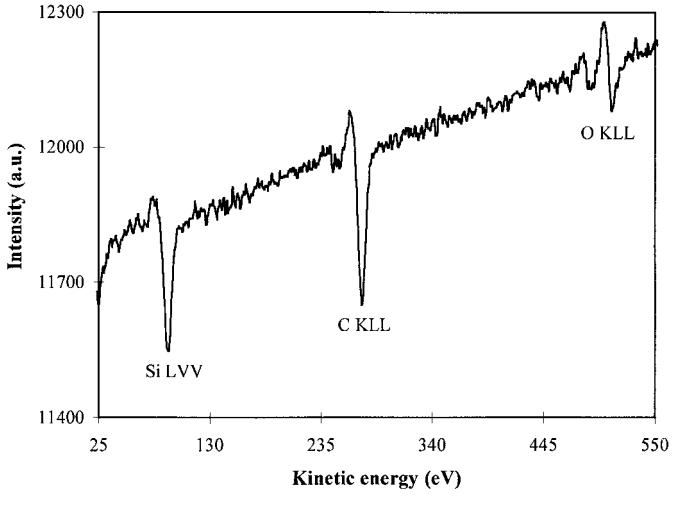

FIG. 2. Auger spectrum of the β-SiC support, after the support was cleaned by argon ion bombardment and annealing.

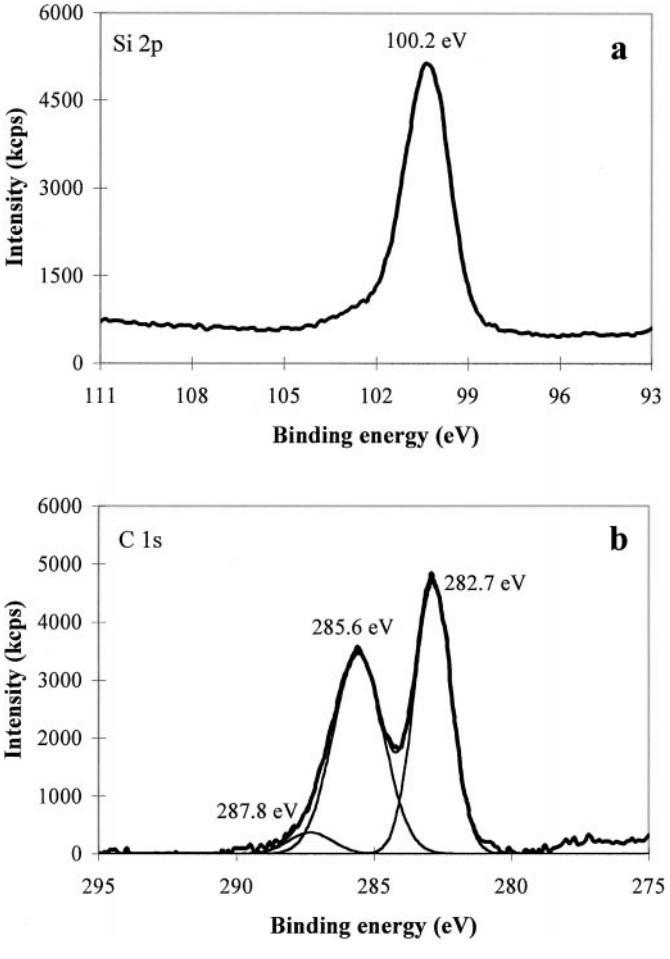

FIG. 3. Si 2p (a) and C 1s (b) XPS spectra for SiC support.

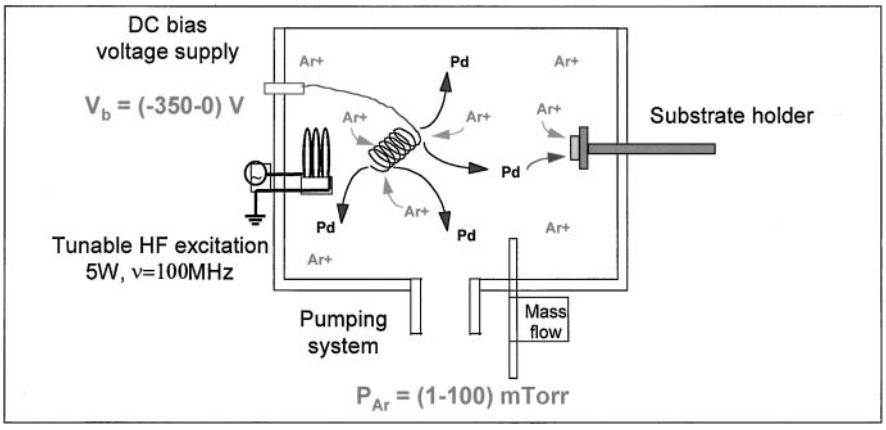

FIG. 4. Plasma sputtering deposition reactor.

energy to induce sputtering (7). The deposition process on the substrate takes place several centimeters away from the wire. During deposition, the SiC surface is subject to the action of energetic plasma species (electrons, metastable atoms, ions) and to UV irradiation. The ions are expected to play a major role in the metal growth mode. They are able to create defects on the substrate surface which may act as preferential anchoring sites for incoming metal atoms. They may also break the growing clusters or increase the mobility of metal adatoms (at the substrate surface or at the aggregate circumference) and of small clusters (8). Under the present experimental conditions, the ions have a quite low mean energy (several tens of electronvolts), and the ion flux could be estimated to 10^{14} at./cm^2/s. The metal deposition rate was about 2×10^{13} at./cm^2 s, and the energy of the condensing atoms was not more than the thermal energy (0.03 eV). The deposited amount of metal (0.3–12 ML, 1 ML being defined as 1.5×10^{15} at./cm^2) was controlled by the deposition time and measured by ex situ RBS analysis. Three Pd deposits were investigated, PSD 1, PSD 2, and PSD 3; their respective Pd amounts are reported in Table 1.

(c) Pd/SiC Prepared by Metal Atomic Beam Deposition (ABD)

The SiC support was first sputtered clean and heated to 870 K under UHV conditions (base pressure 5×10^{-10} mbar). It was then transferred under vacuum into the preparation chamber (base pressure 2×10^{-9} mbar) equipped with Knudsen cells. The Pd evaporation occurred with a deposition rate of about 2×10^{13} at./cm^2 s; the deposits were controlled by a quartz microbalance calibrated from RBS measurements. The Pd deposition was made on a limited area of the sample (0.64 cm^2) with the help of an 8-mm circular aperture located in front of the SiC support as described elsewhere (9). The amount of deposited Pd was also checked a posteriori by RBS; values are reported in Table 1 in which the samples are labeled as ABD 1, ABD 2, and ABD 3.

TABLE 1

Amounts of Deposited Pd for the Various Catalysts, Determined by RBS (Accuracy: 10%)

Samples	Pd amounts (at./cm^2)		
Pd/SiC	PSD 1	PSD 2	PSD 3
(cold plasma)	(5.2×10^{14})	(5.3×10^{15})	(1.9×10^{16})
Pd/SiC	ABD 1	ABD 2	ABD 3
(atomic beam deposition)	(6.0×10^{14})	(3.5×10^{15})	(8.2×10^{15})

(d) Characterization Techniques

The various Pd/SiC samples were characterized by many complementary techniques: TEM, AFM, GISAXS, XPS, AES.

TEM experiments were performed with a JEOL 2010 microscope working at 200 keV and equipped with a UHR pole piece. Due to their thickness, the samples cannot be observed directly. In order to perform TEM observations the extractive replica method was used (10). A thin carbon film (<100 nm thick) was deposited onto the SiC surface where the Pd had been deposited. Then a solution concentrated in hydrofluoric acid (HF) was used to remove the support (SiC) so that a carbon film containing the Pd particles could be obtained (extractive replica). Since silicon carbide is chemically inert, its reaction with HF is unlikely. We think that the presence of a slight surface oxidation (due to air exposure) allows the HF solution to dissolve the outermost layer so that the extractive replica can be obtained. Furthermore, it has been shown recently that RBS experiments induce a swelling of the SiC surface without chemical modification (11). The swelling undoubtedly weakens regions in the carbon film, allowing the HF solution to reach the SiC outermost layer. In this way we succeeded in making the extractive replica on the RBS analysis region for

Pd/SiC samples obtained by PSD. But, it was not possible to extract the Pd particles for catalysts prepared by ABD. This will be discussed later.

The morphology of the Pd particles was also determined tentatively using AFM experiments performed in air with a Nanoscope III Multimode (Digital Instruments Inc., Santa Barbara, CA). In these experiments, we used AFM in the tapping mode (TMAFM) where the tip oscillates at high frequency (≈300 kHz) and comes into contact with the surface at each oscillation. When the tip is scanned over the surface (or vice versa, as is actually the case for the Nanoscope III), modifications of oscillation amplitude are induced by surface height variations. A feedback loop is used to adjust the amplitude variation and to keep the set-point stable, thus yielding a topographic image (12). Moreover, as the tip is not in contact with the surface continuously, frictional forces and sample damage are reduced to a negligible level, and particles physisorbed on surfaces can be visualized without being displaced. Si tips with a typical 10-nm curvature radius were used.

Small-angle X-ray scattering was also carried out on the deposits. Details of this experiment, performed at the LURE laboratory with a synchrotron X-ray source, can be found in Ref. (13). This analysis allows us to detect the presence of aggregates on the surface and to determine their mean diameter (d), height (h), and correlation length (l_c, the distance between the centers of two scattering clusters). This statistical information is obtained over about 10^{10} aggregates.

The photoemission XPS experiments were carried out in an ESCALAB 200R machine from Fisons Instruments using the Mg $K\alpha$ line (1253.6 eV). For the catalysts obtained by atomic beam deposition in the UHV chamber, the samples were checked before and after metal deposition by AES using a cylindrical mirror analyzer (CMA) from Riber SA. The AES spectra were recorded with a primary energy of 1500 eV and a modulation amplitude of 4 V_{pp}.

The 1,3-butadiene hydrogenation was used as a test reaction for the chemical reactivity of the various samples. The reaction was carried out at room temperature with a butadiene/hydrogen ratio of 5 under a total pressure of about 20 Torr (36.66 mbar). The catalytic measurements were performed in a low (265 cm^3)-volume reactor in the static mode. The Pd/SiC samples were introduced in the reactor which was evacuated up to the complete degassing of the catalysts (pressure less than 10^{-8} mbar). In some experiments (with Pd/SiC samples prepared by atomic beam deposition), the catalysts were transferred into the reactor under UHV conditions in order to check that the results are not changed when the transfer occurs under air atmosphere. The course of the runs was followed by analysis with a mass spectrometer, located in the UHV chamber, the reaction mixture being introduced in the chamber through a leak valve. With this type of analysis, it is not possible to separate the three isomers of butene. Therefore, to this aim, the reaction gases were introduced through a valve into a small volume (<3 cm^3) equipped with a septum. They were sampled with a syringe (1 ml) through the septum and analyzed separately by gas chromatography (stainless steel column, 7 in. × 1/8 in., 0.19% picric acid on Graphpac GC, 80/100). The number of chromatographic analyses (<10) was limited so that the reaction rate was not disturbed by the pressure change in the reactor.

RESULTS

Before the catalytic performances of the catalysts prepared either by PSD or by ABD are compared, the main characteristics of the Pd deposits (morphology, electronic properties, etc.) are presented.

The XPS spectra (Pd $3d_{5/2}$ level) recorded for the catalysts prepared by both techniques are reported in Figs. 5a and b. For samples PSD 2 and PSD 3, with the two largest amounts of Pd, the binding energy (BE) of the Pd $3d_{5/2}$ level, ≈335.4 eV, corresponds to the value generally accepted for pure bulk palladium (14). For sample PSD 1, containing the lowest amount of Pd, the Pd 3d binding energy is shifted toward higher values; the corresponding XPS spectrum can be decomposed into two peaks centered at 336.3 and 338.2 eV (mean position at ≈337 eV given in Fig. 5a), which indicates that the very first Pd adatoms interact rather strongly with the SiC support or that their morphology is quite peculiar (15), which will be discussed in the following. This behavior has been confirmed for a lower content (1.5×10^{14} at./cm^2) Pd sample (PSD 0). The binding energy of the Pd $3d_{5/2}$ level is also high (336.6 eV) for the low-content ABD Pd samples. It remains quite high (336.3 eV) even for 2 and 6 ML. This can be due to some support effect or to a specific low dimensionality of Pd particles (small size of metal particles or very thin layers of Pd laid on SiC) (15).

The TMAFM and TEM images of the catalysts obtained by PSD are shown in Figs. 6 and 7, respectively, and the TEM, TMAFM, and GISAXS results for these samples are given in Table 2.

Since in AFM (and TMAFM), from the geometric point of view, the image is formed by a tip contribution and a surface contribution, the lateral resolution will be limited by the tip geometry. Consequently, we have taken into account the geometric contribution of the tip (as defined earlier) and made the necessary correction (16) for the determination of the diameter of the particles. However, as long as the tip is able to reach the substrate surface between adjacent particles, the height can be measured directly by these techniques with good accuracy. The sample PSD 1 image (Fig. 6b) shows clearly the presence of large "particles" with sizes around 6.5 nm but only 1.5 nm height (Table 2). Images of samples PSD 2 (Fig. 6c) and PSD 3 (Fig. 6d) only show the presence of a rough layer all over the surface. This

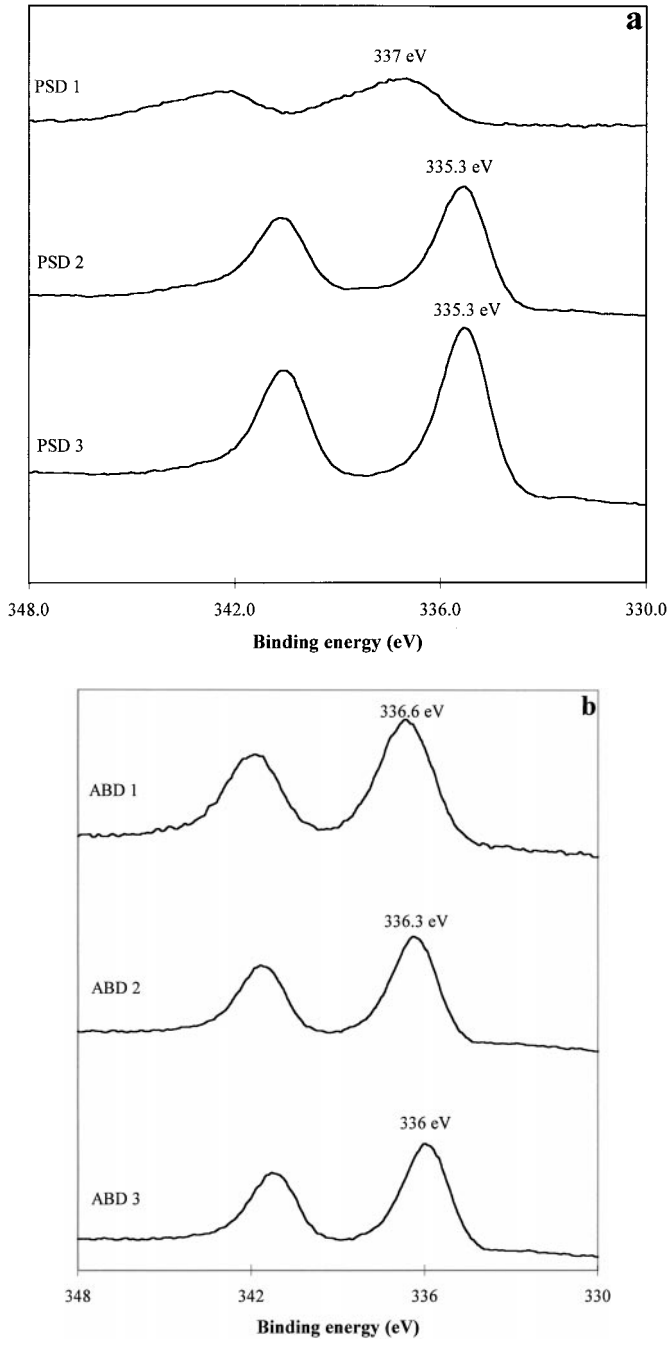

FIG. 5. Pd 3d XPS spectra for the PSD samples (a) and for the ABD samples (b).

rough layer appears to follow the surface topography since the grooves detected on the SiC surface prior to deposition (Fig. 6a) are still clearly visible.

TEM results obtained from the analysis of the three images shown in Fig. 7 are reported in Table 2. The measure of the fraction of surface covered by palladium allows an estimation of the mean height of the Pd particles to be made by taking into account the quantity of Pd deposited as obtained from RBS. In sample PSD 1 (Fig. 7a) small individual particles are observed. They do not appear to be randomly distributed on the support since regions completely free of particles are evidenced. A large-scale observation of the particles shows that they seem to have nucleated and grown near morphologic defects (grooves, etc.). The particles appear to be spherical with a diameter of 1.8 nm. The height deduced from TEM (2.0 nm) is close to that measured by TMAFM (1.5 nm). The diameter measured by TEM (1.8 nm) and that obtained by TMAFM (6.5 nm), after the correction for tip contribution, do not agree. This is not surprising since we can see that, in the regions where particles are observed, the distances between particles are much less than 10 nm (Fig. 7a), which prevents the tip (curvature radius $\approx$10 nm) from reaching the substrate surface between the particles. So the measurement given by TMAFM is related to groups of particles and not to individual ones. In sample PSD 2 (Fig. 7b) the particles are randomly distributed on the surface, and some coalescence is observed. In sample PSD 3 (Fig. 7c) the particles have grown to form meandering islands which are interconnected. In both cases the distances between particles are much smaller than 10 nm. This explains why the TMAFM images show a rough layer superimposed on the SiC topography.

Further characterization by GISAXS was carried out on PSD 1, PSD 2, PSD 3, and ABD 2 samples, giving some complementary information for sample PSD 2. On the first sample no signal was detected, maybe because the deposited metal quantity is too low. For sample PSD 2 the value of the height agrees well with that deduced from TEM. The distance between particles d_i, obtained in TEM (3.0 nm), which corresponds to the value $(l_c - d)$, deduced from GISAXS (2.7 nm), is reliable. The largest value obtained for d may be explained by the fact that GISAXS spectra analysis tends to yield larger than real particle diameters when the size distribution is not isotropic (13), as observed in Fig. 7b. Nothing was observed on ABD 2, although it contains the same amount of metal as PSD 2. This will be commented on in the following discussion. Scattering was observed on sample PSD 3, but the interpretation of the spectrum was not so easy. It seems, however, that large aggregates (gyration radius of about 5.3 nm) are present on the surface, but they do not seem to be correlated. Regarding the morphology evidenced by TEM on this sample, the obtention of a diffuse scattering spectrum is not surprising. Indeed, one of the GISAXS limitations is that it requires compact shape aggregates with a narrow size distribution to be effective (17).

Results given in Table 2 show rather good agreement between the values obtained by the three physical characterization techniques, with only very slight discrepancies that have been discussed. Further information concerning the morphology of metal particles, on either the PSD or the ABD samples, can be deduced from the I_{Pd3d}/I_{Si2p} ratios of the related XPS peak areas. Assuming layer-by-layer

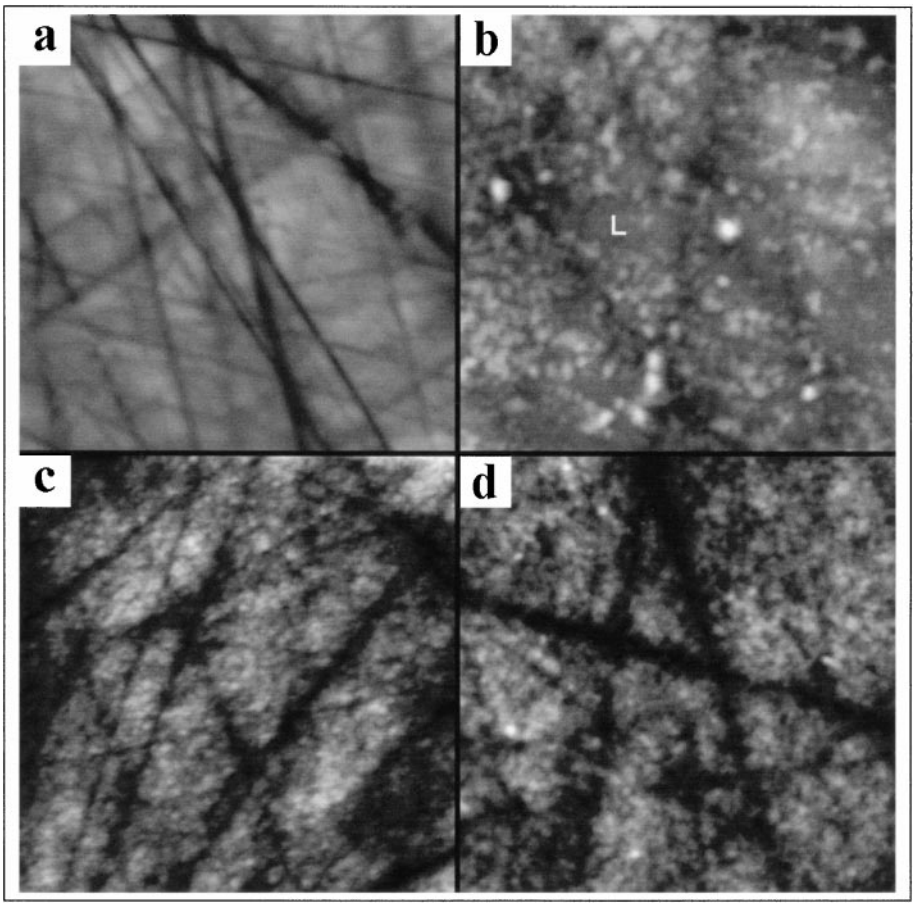

FIG. 6. TMAFM images (500 nm × 500 nm) of the SiC surface (a) and samples PSD 1 (b), (L denotes a region without particles), PSD 2 (c), and PSD 3 (d). *Z* range is 10 nm (black to white) for all images.

growth the number of deposited monolayers on each sample can be calculated and compared to the Pd amounts known from RBS measurements. The results are given in Table 3.

One can see that the layer-by-layer model fits rather well for the Pd adlayers prepared by ABD but fails as soon as the Pd content is above a few fractions of a monolayer for the samples obtained by PSD.

Whatever the sample, the hydrogenation gives only butenes up to the complete disappearance of 1,3-butadiene according to the reaction pathway:

$$\text{1,3-butadiene} + H_2 \Leftrightarrow \text{butenes} + H_2 \Leftrightarrow \text{butane}$$

Typical curves of C_4H_6 and reaction products' pressures versus the reaction time are given in Fig. 8a. The

TABLE 2

Main Characteristics of Metal Particles Produced by Plasma Sputtering Deposition Deduced from TMAFM, TEM, and GISAXS Measurement, i.e., Mean Diameter, *d*, and Height, *h*, Fraction of Surface Covered by Pd, θ, Correlation Length, l_c, and Distance, d_i, between Particle Sides

	TMAFM results		TEM results				GISAXS results		
Sample	*d* (nm)	*h* (nm)	θ (%)	*d* (nm)	*h* (nm)	d_i (nm)	*d* (nm)	*h* (nm)	l_c (nm)
PSD 1	6.5[a]	1.5 ± 0.3	3.7	1.8 ± 0.2	2.0	—	—	—	—
PSD 2	—	—	33	2.3 ± 0.2	2.4	3.0 ± 0.2	3.4 ± 0.4	2.4 ± 0.4	6.1 ± 0.4
PSD 3	—	—	82	4–5[b]	3.5	1.2 ± 0.2	—	—	—

[a] See the text for comments on this value.
[b] This value corresponds to the width of the meandering islands forming the quasi-continuous film.

TABLE 3

Comparison between the Number of Monolayers of Deposited Metal Deduced from the RBS (in Equivalent Monolayers) and XPS Measurements (1 ML $\approx 1.5 \times 10^{15}$ at./cm^2)

Sample	RBS (at./cm^2)	RBS (no. of ML)	XPS (I_{Pd3d}/I_{Si2p})	XPS (no. of ML)
PSD 0	1.5×10^{14}	0.1	0.2	0.09
PSD 1	5.2×10^{14}	0.37	0.5	0.22
PSD 2	5.3×10^{15}	3.5	3.8	1.62
PSD 3	1.9×10^{16}	12.7	very high value	large uncertainty
ABD 1	6.0×10^{14}	0.4	1.0	0.45
ABD 2	3.5×10^{15}	2.3	4.1	1.73
ABD 3	8.2×10^{15}	5.4	high value	poor accuracy

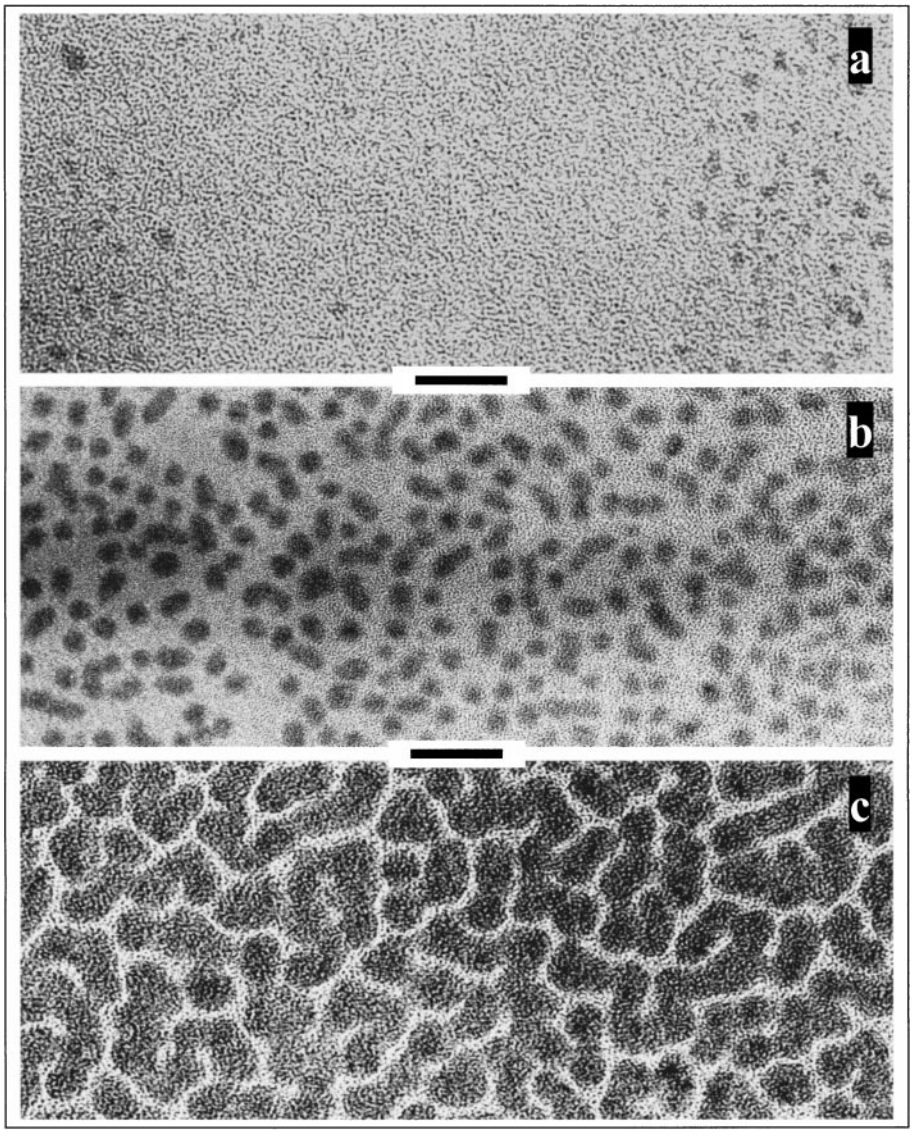

FIG. 7. TEM images of the extractive replicas obtained for samples PSD 1 (a), PSD 2 (b), and PSD 3 (c). Scale bars are 10 nm.

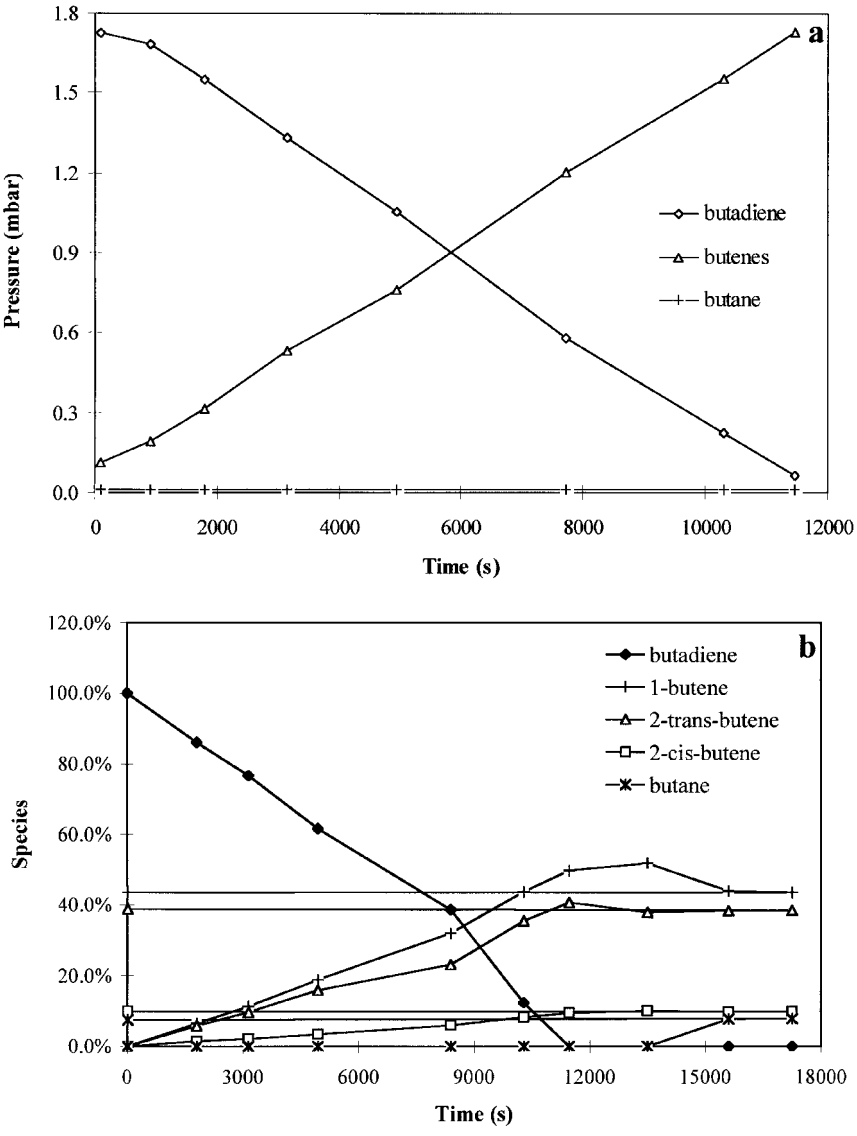

FIG. 8. Reactivity results: (a) Typical curves of butadiene and reaction products' (butenes, butane) pressure versus the reaction time. (b) Evolution of the reaction products (butene isomeres and butane) during the 1,3-butadiene hydrogenation. (c) Selectivity toward the different butenes as a function of butadiene conversion.

catalytic results are gathered in Table 4. The turnover frequencies are calculated on the various samples assuming zero order with respect to C_4H_6, one order with respect to H_2 (18), and the number of surface Pd atoms (exposed to the reacting gases) deduced from the morphology of the Pd deposit. This was performed by either considering a layer-by-layer growth for ABD films or using the particle sizes determined by TEM for the samples prepared by PSD.

The selectivities for the different butenes formed are gathered in Table 5 for the most active catalysts. The results are given at half-conversion of butadiene and at nearly complete disappearance of butadiene. No significant differences are monitored whatever the preparation method, 2-*cis*-butene is always the minor product, and the amount of 1-butene formed is slightly higher than the quantity of 2-*trans*-butene (see Fig. 8c).

TABLE 4

Activity of the Samples for 1,3-Butadiene Hydrogenation

Sample	Activity (molecules cm^{-2})	Dispersion[a]	n_s[b]	TOF (s^{-1})
PSD 1	3.6×10^{12}	0.63	3.3×10^{14}	0.011
PSD 2	9.5×10^{13}	0.49	2.6×10^{15}	0.036
PSD 3	1.5×10^{15}	0.23	4.4×10^{15}	0.34
ABD 1	1.4×10^{14}		5.8×10^{14}	0.24
ABD 2	4.8×10^{14}		1.5×10^{15}	0.32
ABD 3	2.1×10^{15}		1.5×10^{15}	1.4

Note. The TOF are calculated for 10 Torr (13.33 mbar) of hydrogen pressure.

[a] For plasma samples, the dispersion is calculated from TEM results.

[b] n_s is the number of outer Pd atoms calculated on the basis of the number of deposited Pd atoms measured by RBS and either the dispersion (for PSD) or assuming a layer-by-layer growth (for ABD).

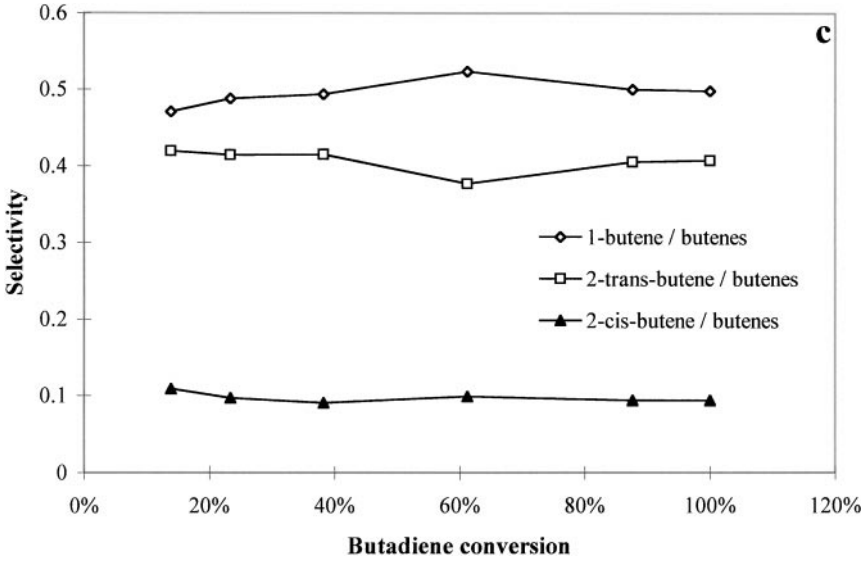

FIG. 8—*Continued*

DISCUSSION AND CONCLUSION

A relatively good description of the morphology of the samples obtained by both methods has been derived from the comparison, and rather good agreement, of the results obtained with different characterization techniques (TMAFM, TEM, GISAXS) together with XPS measurements. All techniques show that the plasma-deposited Pd is composed of more or less 3D Pd particles even for the under-monolayer deposits. A nucleation and cluster growth step is observed, followed by a coalescence phenomenon leading to meandering islands. These islands, clearly visible on sample PSD 3, are composed of elementary "clusters" of about 4–5 nm. This kind of morphology has been evidenced already in the case of Pd deposited on SiO_2 native oxide or amorphous carbon by the plasma sputtering method (19, 20). It has also been reported for metal thin film growth on amorphous or ionic substrates by vacuum deposition at room temperature (21, 22). It is seen from the results in Table 2 that the cluster diameter and, thus the metal coverage, increases with the metal content, as expected.

For ABD samples all results tend to show that layer-by-layer growth occurs. This is further confirmed by the impossibility of obtaining GISAXS results for ABD 2, which indicates that the morphology is particular, i.e., different from well-dispersed 3D islands.

These conclusions agree with the comparison established in Table 3 between the number of monolayers of deposited Pd measured from RBS (in equivalent monolayers) and the XPS determinations. Indeed, the attenuation of the I_{Pd3d}/I_{Si2p} ratio with the Pd content can be related to the thickness of the deposit depending upon the growth mode: layer-by-layer or adaggregates. At very low coverage, the layer-by-layer model used to estimate the number of Pd monolayers from the XPS ratio is valid whatever the preparation method, because no difference depending on the regime can be evidenced at the very beginning of the growth. For higher Pd contents, layer-by-layer growth for ABD is still valid, whereas a clear departure from this law is observed for PSD deposits, which can be attributed to 3D aggregate growth. This is clearly supported by the measure of the I_{Pd3d}/I_{Si2p} ratio (Table 3) for the $(5.2–6) \times 10^{14}$ at./cm^2 samples. This ratio for the PSD sample is half that for the ABD sample, showing a stronger attenuation of the substrate signal when the morphology is 2D island compared with 3D growth. The very high intensity ratio obtained for thicker layers in both cases, i.e., the very low signal characteristic of the SiC substrate, indicates that the Pd tends to

TABLE 5

Selectivities for the Different Butenes for Samples PSD 3 and ABD 3

	1-butene/butenes		2-*trans*-butene/2-*cis*-butene	
Sample	half-conversion	≈90% conversion	half-conversion	≈90% conversion
PSD 3	0.51	0.50	4.2	4.3
ABD 3	0.67	0.69	4.4	4.6

spread all over the surface of the support when its thickness increases, even in the case of 3D aggregate PSD deposits. These observations qualitatively drawn from XPS analyses are in good agreement with TEM, TMAFM, and GISAXS results.

The higher binding energies of the Pd 3d XPS peak measured on ABD 1, ABD2, ABD3, and PSD 1 samples, compared to the values generally accepted for pure Pd (14), are consistent with a palladium adlayer made up of very small metal particles or flat islands. On PSD samples, it can be assumed that the binding energy upward shift is explained mainly by the small size of Pd particles for low Pd amount; the effect disappears completely when the Pd content increases, i.e., when the particle size increases as evidenced by TEM. The Pd atoms exhibit then the same electronic properties as the bulk metal. For ABD samples the low dimensionality along the normal of the SiC support surface, which is retained up to at least 6 ML Pd deposit, can explain the higher Pd 3d binding energy. In other words a rather strong support interaction exists. The fact that it has not been possible to unstick the metal particles on these samples to make extractive replicas for TEM observations is in good agreement with the presence of a more strongly interacting adlayer.

A schematic representation of the proposed morphology of the adlayer depending upon the Pd content and the method of preparation is presented in Fig. 9.

With respect to their catalytic reactivities, all the samples studied show the same selectivity, leading to butenes. The butenes distribution depends slightly on the nature of the Pd coating, PSD or ABD method, but in all cases 1-butene and 2-*trans*-butene dominate (Table 5).

The samples with the lowest metal content prepared by the PSD method are the less active materials; the PSD 1 catalyst is more than 1 order of magnitude less active than Pd(111) which exhibits, in such conditions, a TOF of $\approx 0.28\ s^{-1}$ (23). The rather low activity is most certainly explained by the specific morphology of these samples together with the important binding energy shift recorded for the Pd 3d XPS peak. The more probable explanation is that a rapid deactivation process occurs, as observed on very small Pd particles deposited on graphite, as long as they show an upward shift of their electronic core levels' binding energies (24).

It is clear that the activity increases with the Pd content, and the PSD 3 sample is at least as active as Pd(111). This result shows that the plasma method is efficient in preparing active catalysts.

The activity of the ABD samples ranges between that of the Pd(111) (TOF of about $0.28\ s^{-1}$) and that of the Pd(110) (TOF of about $2\ s^{-1}$) (23). A noticeable activity is measured even for the lowest Pd deposit (sample ABD 1). But again the activity increases with Pd coverage, and a value of $1.4\ s^{-1}$ is calculated for the sample ABD 3. However, such a value could be an overestimate since there is some doubt about the estimation of the number of outer Pd atoms. It is a priori difficult to draw a safe relationship between the structure, the support interaction, the BE shift, and the reactivity. Nevertheless, one can again remark that the TOF increases as soon as the Pd 3d BE decreases, i.e., when the Pd coverage is increased. An epitaxial strain effect, as postulated for Pd deposits on SiC (0001) (9) prepared in the same way as the ABD samples (UHV treatment, Ar^+ ion bombardment, and Pd atomic beam deposition), could explain the decrease of the BE chemical shift with metal coverage through some relaxation of strains. In other words, the Pd–support interaction is probably lower for thicker layers.

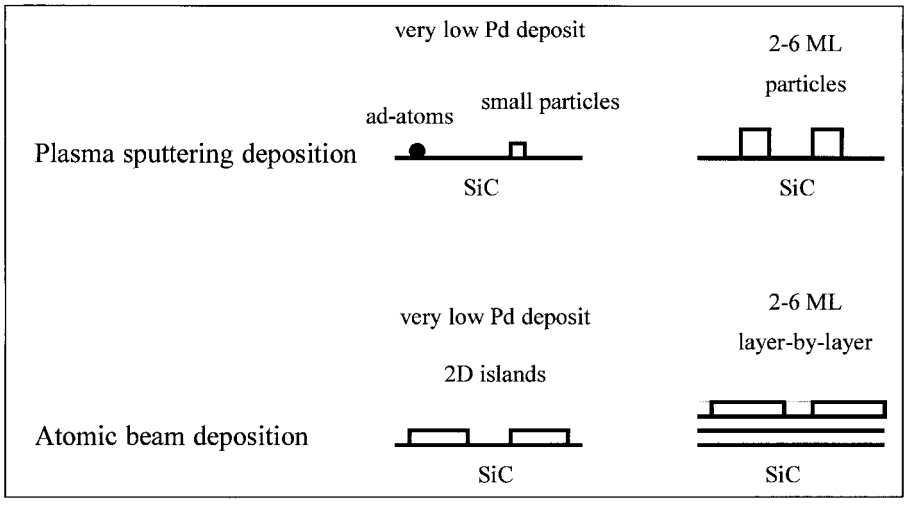

FIG. 9. Schematic representation of the growth process proposed for the two methods of preparation: plasma sputtering deposition (PSD) and atomic beam deposition (ABD).

In conclusion, active catalysts composed of very thin metal adlayers on flat supports can be prepared by atomic beam deposition but also by low-pressure plasma sputtering deposition. The morphology of the metal adlayer depends upon the physical deposition method used.

Palladium deposits obtained by ABD interact strongly with the SiC support and grow in a rather uniform layer-by-layer mode. The morphology of palladium adlayers prepared by PSD is different. First, very small aggregates are formed, and embedded metal atoms and/or atomically dispersed Pd could be present at the surface. Larger particles grow to finally coalesce and form meandering islands. The physical effect of Ar^+ ion bombardment, which occurs during the metal deposition, can generate many kinds of defects on the substrate and/or influence the condensing metal atom mobility. By modifying the plasma parameters, the deposition conditions (incoming ion flux and energy, condensing metal atoms flux and energy) can be monitored, and consequently the number of created anchoring sites and/or the cluster growth evolution can be varied. The present study shows that the plasma sputtering deposition technique is a promising method for obtaining finely controlled metal deposits that can be used as catalysts.

REFERENCES

1. Methivier, Ch., Beguin, B., Brun, M., Massardier, J., and Bertolini, J. C., *J. Catal.* **173**, 374 (1998).
2. Tardy, B., Noupa, C., Leclercq, C., Bertolini, J. C., Hoareau, A., Treilleux, M., Faure, J. P., and Nihoul, G., *J. Catal.* **129**, 1 (1991).
3. Laure, C., Brault, P., Thomann, A. L., Boswell, R., Rousseau, B., and Estrade-Szwarckopf, H., *Plasma Sources Sci. Technol.* **5**, 510 (1996).
4. Muehlhoff, L., Choyke, W. J., Bozack, M. J., and Yates, Jr., J. T., *J. Appl. Phys.* **60**, 2842 (1986); Hornetz, B., Michel, H. J., and Halbritter, J., *J. Mater. Res.* **9**, 3088 (1994).
5. Johansson, L. I., Owman, F., and Mårtensson, P., *Phys. Rev. B* **53**, 13793 (1996).
6. Van Bommel, A. J., Crombeen, J. E., and Van Tooren, A., *Surf. Sci.* **48**, 463 (1975); Parrill, T. M., and Chung, Y. W., *Surf. Sci.* **243**, 96 (1991).
7. Thomann, A. L., Charles, C., Brault, P., Laure, C., and Boswell, R., *Plasma Sources Sci. Technol.* **7**, 245 (1998).
8. Chambers, G. P., and Startwell, B. P., *Surf. Sci.* **218**, 55 (1989).
9. Lianos, L., Berthet, A., Deranlot, C., Cadete Santos Aires, F. J., Massardier, J., and Bertolini, J. C., *J. Catal.* **177**, 129 (1998).
10. Gallezot, P., and Leclercq, C., *in* "Catalyst Characterization. Physical Techniques for Solid Materials" (B. Imelik and J. C. Védrine, Eds.), p. 509 Plenum, New York, 1994.
11. Fukarek, W., Yankov, R. A., Anwand, W., and Heera, V., *Nucl. Instrum. Methods. Phys. Res. B* **142**, 555 (1998).
12. Zhong, Q., Inniss, D., Kjoller, K., and Elings, V. B., *Surf. Sci. Lett.* **290**, 688 (1993).
13. Thiaudière, D., Thèse de Doctorat, University of Poitiers, 1992.
14. Jones, M. G., Newell, T. G., Ewen, R. J., and Honeybourne, C. L., *Appl. Catal.* **70**, 277 (1991); Otto, K., Haack, L. P., and De Vries, J. E., *Appl. Catal. B* **1**, 1 (1992); Bertolini, J. C., Delichère, P., Khanra, B. C., Massardier, J., Noupa, C., and Tardy, B., *Catal. Lett.* **6**, 215 (1990).
15. Kohiki, S., *Surf. Sci.* **25**, 81 (1986).
16. Soffray, C., DEA Diploma, University Claude Bernard Lyon I, 1995. Deranlot, C., DESS Diploma, University of Poitiers, 1997.
17. Naudon, A., and Thiaudiere, D., *Surf. Coatings Technol.* **79**, 103 (1996).
18. Massardier, J., Borgna, A., Ouchaib, T., Moraweck, B., and Renouprez, A. J., *in* "12° Simpósio Ibero-Americano de Catálise, Trabalhos Técnicos" (Comissão de Catálise, Ed.), Vol. 1, p. 529 IBP/CAT, Rio de Janeiro, 1990.
19. Thomann, A. L., Brault, P., Rozenbaum, J. P., Andreazza-Vignolle, C., Andreazza, P., Estrade-Szwarckopf, H., Rousseau, B., Babonneau, D., and Blondiaux, G., *J. Phys. D: Appl. Phys.* **30**, 3197 (1997).
20. Brault, P., Thomann, A. L., and Andreazza-Vignolle, C., *Surf. Sci.* **406**, 597 (1998).
21. Evans, B. L., Maaroof, A. I., and Xu, S., *J. Appl. Phys.* **76**, 900 (1994).
22. Heim, K. R., Coyle, S. T., Hembree, G. G., Venables, J. A., and Scheinfein, M. R., *J. Appl. Phys.* **80**, 1161 (1996).
23. Massardier, J., Bertolini, J. C., and Renouprez, A. J., *in* "Proceedings of the 9th International Congress on Catalysis" (M. J. Phillips and M. Ternan, Eds.), Vol. 3. p. 1222. Chem. Institute of Canada, Ottawa, 1988.
24. Noupa, C., Rousset, J. L., Tardy, B., and Bertolini, J. C., *Catal. Lett.* **22**, 197 (1993).